OTC 6364

Experimental Study of Kinematics of Large Transient Wave in 2-D Wave Tank

C.H. Kim, R.E. Randall, M.J. Krafft, and S.Y. Boo, Texas A&M U.

This paper was presented at the 22nd Annual OTC in Houston, Texas, May 7–10, 1990.

ABSTRACT

Increased attention has recently been focused on determination and reproduction of realistic properties of extreme sea waves for use in numerical and physical modeling and design load computations. Results of recent research on laboratory synthesis of extreme waves and experimental investigation of wave-fluid particle kinematics just prior to breaking using laser Doppler anemometry is presented. An extreme transient wave, similar to those found in hurricane Camille, and an "equivalent" regular Stokes wave often used for design purposes were generated, and their kinematics measured. Due to particular asymmetries not present in the Stokes wave, the transient wave kinematics under the crest are shown to be much more severe above the still water level and somewhat less severe below. This comparison suggests that it would be worthwhile to further investigate the use of extreme, transient waves as new, more realistic design waves.

INTRODUCTION

Offshore structures are diverse in their configurations, sizes and modes of moorings/fixings. Natural sea environments consisting of winds, currents and waves acting on and interacting with structures produce complex fluid loadings that are difficult to evaluate. However, practical techniques have been established for estimating wave loads under limited conditions, such as the Morison equation for slender bodies and diffraction theory for large structures. Morison's equation requires determination of inertia and drag coefficients and knowledge of the fluid kinematics resulting from wave and current interaction under the wave surface, in the absence of any structure.

It is usual practice in determining wave kinematics to follow either a random wave or deterministic design-wave approach. The random wave (time series) is obtained from the energy spectra of design sea state, whereas the design wave (characterized only by height and period) is derived statistically as the most probable, largest wave at the design location for a given return period. Random wave approaches, for instance [1, 2, 3], use linear wave theory and the linear random superposition law and develop empirical formulas for determining the particle kinematics above the mean water level, using so called "stretching" techniques. The design wave can be represented by a variety of wave theories [4] including Airy, Stokes, cnoidal, stream function, etc. Consequently, in using the foregoing wave theories, a number of particle kinematics data are generated and lead to estimates of design wave loads.

Recent progress in gathering and analyzing storm sea surface data, for instance [5, 6, 7], has resulted in a significant impact on those in the research community interested in studying extreme waves and wave loadings on marine structures. For example, an analysis of data from the Gulf of Mexico hurricane "Camille" and a storm off the Irish coast [6] revealed that some of the largest waves contained in sample time histories were steep on their forward face and greatly elevated. Such waves are often termed extreme transient waves.

Extreme transient waves have been reproduced in a few wave tanks, for instance [8-14, 17]. Kinematic measurements of extreme waves made by Kjeldsen et al [9, 13] with electromagnetic current meters indicated crest velocities 36% greater than phase velocity just prior to breaking, and prompted them to propose that combinations of severely asymmetric transient waves be selected as design waves, in order to avoid severe under-estimation of wave loads.

Studies of the kinematics of breaking waves by Dommermuth et al [14] employed a potential theory for predicting wave elevation and velocity and used laser Doppler anemometry (LDA) to measure fluid velocities under the wave surface including the region above the

References and illustrations at end of paper.

mean water level. Numerical results from the potential theory compared well with the laboratory experiments. Birkinshaw, et al [15] investigated the kinematics of spilling breakers for the design of a small offshore gas platform. Using LDA to measure velocities in the wave crest, they found that values predicted from stream function wave theory were exceeded by 20%. Skjelbreia [16] measured extensively by LDA, fluid velocities under solitary waves breaking on a sloped bottom, and the corresponding accelerations were computed.

One objective of this study was to measure the kinematics under a laboratory generated extreme, transient wave using a laser Doppler anemometer. The second objective was to investigate the differences in kinematic behavior between an extreme transient wave and a regular wave of the type often considered as a "design" wave in preliminary investigations of maximum loads. Accordingly, experimental measurements of particle velocities were conducted under the crest of a severely asymmetric transient wave, and are compared to an experimentally determined wave celerity. A large regular wave, approximating a Stokes 3rd order wave, with similar height and period as the transient wave was also created in the laboratory and kinematic measurements were made and compared with those obtained for the transient wave. Due to particular asymmetries not present in the Stokes wave, the transient wave kinematics are shown to be much more severe in the crest region above the mean water level and somewhat decreased in the region below. This comparison suggests that it would be worthwhile to further investigate the employment of extreme transient waves as new, more realistic design waves.

TRANSIENT WAVE GENERATION

A transient water wave (TWW) may be defined as a wave with finite duration or energy. Mathematically, the TWW can be thought of as a combination of a finite number of linear waves and represented in the frequency domain as a Fourier spectrum. In the laboratory a sequence of relatively small component waves can be generated such that they meet almost simultaneously, and focus their energy at a given time and downstream location. Since linear waves are primarily characterized by their phase and amplitude, successful creation of a well focused TWW depends largely on the control of these characteristics. In the synthesis procedure, the variation in amplitude, frequency and the number of component waves in the resulting time series depends on the design of the Fourier spectrum for the concentrated TWW, the distance from wave maker to test site and the length of the time series.

In addition, the size and type of wave making facilities impose physical limits on the component waves that can be utilized; consequently there must be a limit on the size of the resulting focused TWW. Whether or not that limit can be achieved depends on the degree of control exerted on the driving voltage signal, i.e., dependent upon how well the wave maker transfer functions are described, the order of wave generation used and the appropriate use of complex corrective transfer functions to account for component wave nonlinearities. The present synthesis methodology [11] follows that of Takezawa and Hirayama [12], which emulates the ideas presented by Davis and Zarnick [17], but is further developed with respect to phase and amplitude control of the component waves. Takezawa's controlled synthesis provides for more complete concentration over a relatively shorter duration than previous methods, hence reducing the effects of reflection during model tests. These attributes were considered desirable given the relatively short length (37 m) of the experimental facility in which these tests were to be conducted.

From linear control systems theory, the complex Fourier spectrum for the TWW at a given downstream location (x) has the form:

$$H_x(\omega) = A_{hx}(\omega)\cdot\exp[i\Psi_{hx}] = V(\omega)\cdot G_{hxv}(\omega) \quad \ldots\ldots (1)$$

where $G_{hxv}(\omega)$ is the complex transfer function relating the Fourier spectrum of the driving voltage signal, $V(\omega)$, to the target Fourier spectrum of the wave at the concentration location, x. The total wave making system has been divided into two sub-control systems; one between input voltage amplitude, $A_V(\omega)$, and wave amplitude, $A_{ho}(\omega)$, near the wave maker (x_o=5 m), and the other between wave amplitude near the wave maker and wave amplitude, $A_{hx}(\omega)$, at concentration (x). Accordingly, the transfer function $G_{hxv}(\omega)$ is expanded as:

$$G_{hxv}(\omega) = G_{hov}(\omega)\cdot G_{hxho}(\omega)$$

$$= A_{hov}\cdot A_{hxho}\cdot\exp[-i(\phi_{hov} + \phi_{hxho})] \quad \ldots\ldots (2)$$

Dividing the target wave spectrum by the total transfer function in Eqn. (2) yields the driving voltage spectrum:

$$V(\omega) = [A_{hx}/(A_{hov}\cdot A_{hxho})]$$

$$\cdot\exp[i(\Psi_{hx}+\phi_{hov}+\phi_{hxho})] \quad \ldots\ldots (3)$$

To satisfy the requirement that all component waves concentrate to attain maximum height in a minimum time, the target spectrum phase, Ψ_{hx}, must be an integral multiple of π (i.e., a constant independent of ω) [11] and is arbitrarily set to zero. The phase relation, ϕ_{hxho}, between waves at x_o and x is calculated from linear dispersion, while the amplitude ratio, $A_{hxho}(\omega)=A_{hx}(\omega)/A_{ho}(\omega)$, between these same locations is set to unity, assuming negligible energy loss. The complex transfer function, $A_{hov}\cdot\exp[-i\phi_{hov}]$, between the input driving voltage signal and waves near the wave maker was determined from spectral analysis of a sweep of small amplitude waves covering the frequency range of interest and the corresponding voltage signal. Using the above simplifications, the Fourier voltage spectrum in Eqn. (3) becomes:

$$V(\omega) = [A_{hx}/A_{hov}]\cdot\exp[i(\phi_{hov} + k(x-x_o)] \quad \ldots\ldots (4)$$

The time history of the driving voltage signal is then obtained from the real part of the inverse Fourier transform of $V(\omega)$ in Eqn. (4):

$$V(t) = (1/2\pi)\int \mathrm{Re}\{V(\omega)\cdot\exp(i\omega t)\}\, d\omega \quad \ldots\ldots (5)$$

In the present analysis, an idealized target Fourier spectral model was utilized (Fig. 1) and is based on a

requirement that all component waves have the same predetermined slope as follows:

$$k(\omega,d) \cdot A_{hx}(\omega) = \beta = \text{constant} \quad \ldots\ldots\ldots\ldots\ldots\ldots (6)$$

where $k(\omega,d)$ is the wave number from linear dispersion for a water depth, d.

Fig. 2 shows the elevation time series of the sequence of waves at the upstream reference location of 5 m from the wave maker flap and the resulting focused wave train at the downstream location of maximum concentration of 21.6 m. This particular wave train was designed for maximum concentration at a distance of 20.5 m and time of 50 s. Due to component wave nonlinearities causing small increases in phase speed, the maximum focusing point was shifted downstream slightly, with a focusing time of 49.70 s. The transient wave shown in Fig. 2 was reproduced to prototype scale (1:100) in Fig. 3 (bottom) to illustrate the similarity with a wave selected from hurricane Camille time series data (top). These waves are characterized by their strong asymmetries with respect to both the vertical and horizontal axes. Unlike Stokes type waves, the time series in Fig. 3 and the corresponding wave profiles in Fig. 5 clearly show a greater steepness in the crest front than in the crest rear, a deeper following trough and vertical asymmetry of the troughs themselves.

The focused wave profile computed from the theoretical linear superposition method described can only have Stokes type asymmetries since all components were required to have the same phase at concentration. It is the intentional use of relatively large component waves and the finite depth of water that cause the laboratory transient wave to steepen and exhibit the additional asymmetries seen in Fig. 3 and Fig. 5. In a given wave tank of constant depth, whether or not the TWW breaks before complete concentration, at concentration or at all, depends on the shape and distribution of the design spectrum.

TEST FACILITIES

The experimental measurements were conducted in the two dimensional wave tank located in the Hydromechanics Laboratory in the Civil Engineering Laboratory Building at Texas A & M University. The wave tank is 37 m (120 ft) long, 0.91 m (3 ft) wide and 1.22 m (4 ft) deep and is equipped with a Commercial Hydraulics RSW 90-85 dry back, hinged-flap wave maker and downstream wave energy absorbing beach.

Water particle velocities were measured with a laser Doppler anemometer system. This two-dimensional, three beam laser system, as shown schematically in Fig. 4, consists of an INNOVA 4-watt argon-ion laser and DANTEC optics, mirror and traverse mechanism, and one frequency tracker and shifter for each velocity component. Real time signal monitoring of the two velocity components is provided by data acquisition system (PC-1), employing an IBM PC-XT equipped with an A/D converter board and measurement and processing software. The principal data collection and processing system (DATA ACQ) consists of a Hewlett Packard HP-3852A data acquisition system and HP-330 controller (PC-2). Software was developed for this system to acquire and process LDA system velocity data simultaneously with wave elevation data measured by resistance type wave gauges. The third control system (PC-3) is an IBM PC configured for transmission of the wave maker driving voltage signal.

The present experiments were performed with the wave flap hinge depth equal to the water depth of 0.91 m (3 ft). Acceptable Doppler signals were not attainable without "seeding" the water in and around the test site. The water was seeded with titanium oxide particles about 0.8 microns in diameter to insure the presence of a sufficient amount of suspended solid material to scatter the laser light.

The wave gauge array used to measure water surface elevations was installed in the vicinity of the focusing point where the kinematic measurements were made (Fig. 4). The accuracy of the wave gauges is ± 0.1 cm. A model length scale of 1:100 was utilized in the synthesis of the waves tested.

KINEMATIC MEASUREMENT PROCEDURES

Durrani and Greated [18] and Durst [19] describe laser Doppler anemometer theory and techniques in detail. However, the techniques or procedures as they apply to the present research are now summarized. An argon-ion laser beam is directed into the laser optics where it is split into three beams; a blue beam with a wavelength of 488 nanometers (nm), a green beam with a wavelength of 514.5 nm, and a cyan reference beam. Laser optics equipment includes a 600 mm focal length lens which causes the three beams to intersect at a single "point", known as the probe volume. A mirror and traverse mechanism are used to precisely position the probe volume inside the tank at a sufficient distance away from the side wall boundary and vertically between the water surface and tank bottom. The laser system is mounted on a movable hydraulic bench, permitting lateral movement of the system parallel to direction of wave propagation.

The intersection of the cyan reference beam with the blue and green beams give the vertical and horizontal velocity components respectively. Beam intersections produce a fringe pattern in the probe volume and as the seeding particle, traveling at the same velocity as the water, passes through the fringes it scatters the laser light. The backscattered light is detected by photomultiplier tubes which output a voltage related to the Doppler frequency of the backscattered light. This signal is processed by the frequency tracker and output as an analog voltage signal to the data acquisition system. The Doppler frequency (f) is directly related to velocity (u) by:

$$u = f\lambda / [\, 2 \cdot \sin(\theta) \,] \quad \ldots\ldots\ldots\ldots\ldots\ldots (7)$$

where λ is wavelength of laser beam and θ is the half angle of the intersection of the beams.

The LDA system is aligned prior to the start of measurements to insure coincident intersection of the three laser beams at one point (probe volume). The photomultiplier tubes are focused on the probe volume using pinhole adjustments, and the tracker frequency and filter ranges are set. The zero velocity condition was tested by focusing beams on a fixed point on the tank wall. Typical frequency tracking range settings were either 10 to 100 khz or 33 to 333 khz, and the narrowest filter range of

19 or 59 Hz respectively, was selected. The frequency shift for each channel was set to optimize the range of velocities expected and to facilitate measurement of the oscillating flow. A frequency shift of -50 khz was selected for the 10 to 100 khz range and -100 and -200 khz for the 33 to 333 khz range. The accuracy of the velocity measurements is ± 0.005 m/s for the -50 khz shift, ± 0.02 m/s for the -100 khz shift and ± 0.01 m/s for the -200 khz shift. Each frequency tracker indicates whether the tracker is locked-on to a Doppler signal by a solid green indicator light. An oscilloscope is used to monitor the signal from each tracker unit so that fine tuning of the pinhole, tracker gain and filter adjustments can be optimized to give the strongest Doppler signal.

KINEMATIC MEASUREMENTS RESULTS

A large transient wave was generated in the laboratory wave tank. Fig. 5 illustrates six consecutive profiles of the transient wave at times beginning from 49.58 s and ending at 49.78 s from the initiation of the driving voltage signal. The crest height of the transient wave is shown to be 15 cm above the still water level (SWL) at a distance of 21.6 m from the wave flap, which occurred at a time equal to 49.70 s. The last two wave profiles show a second raised portion at 21.9 m due to wave breaking. These profiles clearly indicate the severely asymmetric nature of the wave. The transient wave at T = 49.70 s has a steeper forward face (asymmetry about vertical axis through crest peak) in the direction of propagation, an elevated crest of nearly 15 cm, a shallow 4 cm leading trough and a 10 cm following trough (horizontal asymmetries). The difference in crest and trough periods is another significant vertical asymmetry. Extreme episodic waves with similar shape have been observed in real ocean wave data. For example, one such wave from Hurricane Camille is shown in Fig. 3.

The horizontal and vertical velocity along seven vertical lines spaced 0.1 m apart in the direction of propagation and at depths relative to the SWL of 14, 10, 5, 0, -10, -20 and -30 cm were measured. These measurements are given in Table 1, and presented graphically as a velocity vector plot in Fig. 6. The results indicate a maximum horizontal velocity of 1.47 m/s measured 1 cm below the crest peak. Along a vertical line directly below the crest peak, the horizontal velocity decreased from 1.47 to 0.52 m/s at the SWL and to 0.19 m/s at -30 cm. Horizontal velocities in rear (upstream) portion of the wave varied from 0.94 to 0.10 m/s and in the forward portion from 0.73 to 0.18 m/s.

The vertical velocity did not monotonically decrease with depth below the SWL. A vertical velocity of 0.15 m/s was measured at 14 cm which decreased to 0.05 m/s at 10 cm, then increased to 0.07 m/s at 5 cm and to 0.09 m/s at -10 cm and then decreased to 0.02 m/s at -30 cm. Vertical velocities in the rear of the wave varied from -0.42 to -0.12 m/s with the velocity vectors oriented in the direction of the wave propagation and down. Above the SWL and in the forward portion of the wave, the vertical velocity was also negative which resulted in slightly downward directed velocity vectors as shown in Fig. 6. In the forward portion of the wave and below the SWL, vertical velocities were positive and thus the velocity vector was slightly upward and in the direction of propagation. Kinematic behavior qualitatively similar to this has been observed by Skjelbreia [16].

Time series of the horizontal and vertical velocities measured at points that are 21.6 m from the wave flap are illustrated in Fig. 7 and Fig. 8, respectively. The maximum horizontal velocities at these points are shown to occur very near the wave crest at a time of 49.70 s. Maximum vertical velocity occurred near the crest peak (14 cm), however, maximum values for other depths occurred slightly before 49.70 s (positive maxima) and just after 49.70 s (negative maxima). The vertical velocities are generally small and tend toward zero directly under the crest peak. As the measurements proceeded upwards to the peak of the crest, the number of data points obtained decreased because the laser probe volume was only immersed in the crest for a short time. This short measurement time window compared to the finite time required for the laser system electronics to lock-on to the Doppler frequency, limited velocity measurements to within 1 cm of the water surface for steep crest peaks.

COMPARISON OF TRANSIENT AND STOKES WAVES

A comparison of Stokes 3rd order wave kinematics to extreme, transient wave kinematics was made to show the basic effects of the additional asymmetries found in certain transient waves. A regular wave closely approximating a Stokes 3rd order wave was generated with a wave height of 25 cm and period (1.36 s) similar to the zero upcrossing period of the laboratory transient wave. A time series comparison of the transient, measured Stokes and theoretical Stokes waves is illustrated in Fig. 9. The phase velocity of the theoretical Stokes wave was computed as 2.18 m/s. The phase velocity of the transient wave was found to be 2.29 s, and was computed from a number of time series recorded at 5 cm intervals in the vicinity of maximum concentration. As shown in Fig. 9, the wave heights for the transient and Stokes wave are essentially the same, but the theoretical Stokes wave has a slightly lower crest and deeper trough. The transient wave has a noticeably different trough level preceding and following the wave crest which is typical for large, laboratory generated transient waves and for some of the extreme waves recorded during severe storms.

Velocity measurements were made at the same depths under the regular wave as were made for the transient wave, and the results are illustrated in Fig. 10. At a 14 cm elevation the horizontal velocity under the Stokes wave was measured as 0.80 m/s. This value is only 54% of the value measured at the same location under the transient wave. The measured Stokes wave values at 10, 5, 0, -10, -20, and -30 cm elevations were 72, 98, 98, 121, 132, and 135% of the velocity values measured in the transient waves at the same elevations, respectively. Fig. 10 indicates that velocities above the SWL were considerably higher in the transient wave, and below the SWL were smaller than those in the measured Stokes wave. Theoretical results show values up to the SWL, and the 0.51 m/s theoretical velocity at the SWL is 35% of the transient wave value of 1.47 m/s. This represents a significant difference in the kinematics of the transient wave and the regular Stokes type wave often used in design calculations, and points to the use of such a transient wave for more realistic wave force values.

CONCLUSIONS

Laser Doppler anemometer measurements of the velocity field were successfully completed beneath the crest of a laboratory generated extreme, transient wave having similar size and asymmetric properties as those found in hurricane Camille. The maximum measured velocity was 1.47 m/s at 14 cm above the SWL and directly under the crest peak just prior to breaking. This value is 64% of the measured phase velocity of the transient wave and 184% of the velocity measured at the same elevation under the Stokes wave. A comparison of measurements of a Stokes 3rd wave indicated the horizontal velocities in the 25 cm transient wave were larger in region above SWL to the crest peak. Below the SWL and under the crest peak the velocities in the transient wave were smaller than those measured below SWL in the Stokes wave.

The capability of measuring velocities in a very short time interval as the tip of the wave crest entered and exited the probe volume was demonstrated, and for the particular transient wave tested, measurements were obtained to within 1 cm of the water surface at the crest peak.

Empirical and/or theoretical techniques need to be developed to predict the kinematics under transient waves. Significant empirical developments will require detailed experimental velocity data collection for a range of transient waves, as well as regular waves, just prior to, and after breaking, and the computation of fluid accelerations from the velocity measurements. Results from new and existing theoretical simulation techniques can be compared to experimental data of the type presented here.

Since it is possible to synthesize a variety of transient wave forms with nearly the same pre-breaking height and period, but having distinctly different asymmetric properties and breaking behavior (all depending on the target design spectra, method of synthesis, water depth, etc), the foregoing kinematic observations are of limited significance. While a great deal of effort has been spent on the probabilistic determination of the heights and periods of the largest waves in storms, comparatively little has been devoted to characterizing the statistics of the nonlinearities of such waves. Therefore, while it is both important and possible to reproduce and analyze extreme, nonlinear wave forms in the laboratory, further research is needed to identify which observed wave forms occurring in nature should be modelled. Based on the present findings and those of several recent investigations, design wave analysis for the purpose of estimating maximum loads on offshore structures should include the effects of extreme wave asymmetries.

NOMENCLATURE

x = downstream transient wave focusing location

t = time

$h_x(t)$ = wave elevation @ x (m) from wave maker

ω = wave frequency

$H_x(\omega)$ = complex target Fourier spectrum of $h_x(t)$

$A_{hx}(\omega)$ = target Fourier spectrum magnitude of $h_x(t)$

$\Psi_{hx}(\omega)$ = target Fourier spectrum phase of $h_x(t)$

x_o = transfer function measurement location

$h_{xo}(t)$ = wave elevation @ x_o (m) from wave maker

$A_{ho}(\omega)$ = target Fourier spectrum magnitude of $h_{xo}(t)$

$v(t)$ = wave maker driving voltage signal

$V(\omega)$ = complex Fourier spectrum of $v(t)$

$A_v(\omega)$ = magnitude of Fourier spectrum of $v(t)$

$G_{hxv}(\omega)$ = complex transfer function spectrum relating $H_x(\omega)$ and $V(\omega)$

$A_{hxho}(\omega)$ = ratio of $A_{hx}(\omega)$ and $A_{ho}(\omega)$

$\phi_{hxho}(L)$ = phase difference between waves @ x and x_o

$A_{hov}(\omega)$ = ratio of $A_{ho}(\omega)$ and $A_v(\omega)$

$\phi_{hov}(\omega)$ = phase change between waves @ x_o and wave maker driving voltage signal

d = water depth

$k(\omega,d)$ = wave number

β = constant

u = water particle velocity

f = Doppler frequency

λ = wavelength of laser beam

θ = half angle of intersection of laser beams

ACKNOWLEDGEMENT

The research reported in this paper was conducted for the Offshore Technology Research Center, which is supported in part by the National Science Foundation Engineering Research Centers Program grant #CDR-8721512.

REFERENCES

1. Foristall, G. Z.: "Kinematics of Directionally Spread Waves," *Proceedings ASCE Conference on Directional Wave Spectra Applications*, Berkley, California, (September 1981), 129-166.
2. Vugts, J. H. and Bosma, J.: "Wave Kinematics and Fluid Loading in Irregular Waves," *International Symposium on Hydrodynamics in Ocean Engineering*, Trondheim, Norway, (August 1981).
3. Rodenbuch, G. and Forristall, G. Z.: "An Empirical Model for Random Directional Wave Kinematics Near the Free Surface," *Proceedings 18th Annual Offshore Technology Conference*, Houston (May 1986).
4. Dean, R. G. and Dalrymple, R. A.: *Water Wave Mechanics for Engineers and Scientists*, Prentice Hall Inc., Englewood Cliffs (1984).

5. Ward, E. G.: "Ocean Data Gathering Program- An Overview," *Proceedings 6th Annual Offshore Technology Conference*, Houston (May 1974).
6. Buckley, W. H.: "A Study of Extreme Waves and Their Effects on Ship Structure," *The Ship Structure Committee Report No. SSC-320*, (1983).
7. Buckley, W. H. and Stavovy, A. B.: "Progress in the Development of Structural Load Criteria for Extreme Waves," *Proceedings Extreme Loads Response Symposium, The Ship Structure Committee and the Society of Naval Architects and Marine Eng.*, (1981).
8. Mansard, E. P. D. and Funke, E. R.: "A New Approach to Transient Wave Generation," *Proceedings 18th International Conference on Coastal Engineering*, Cape Town, South Africa, (1982).
9. Kjeldsen, S. P., Vinje, T., Myrhaug, D. and Brevig, P.: "Kinematics of Deep Water Breaking Waves," *Proceedings 12th Annual Offshore Technology Conference*, Houston (1980).
10. Longuet-Higgins, M. S.: "Breaking Waves in Deep and Shallow Water," *Proceedings 10th Symposium on Naval Hydrodynamics*, MIT (June 1974).
11. Krafft, M. J. and Kim, C. H.: "Extreme Transient Water Wave Generation at Texas A&M University," *COE Report 294, Civil Eng. Dept, Ocean Engineering Program, Texas A&M University*, (December. 1987).
12. Takezawa, S., and Hirayama, T.: "Advanced Experimental Techniques for Testing Ship Models in Transient Water Waves: Part II the Controlled Transient Water Waves for Using in Ship Motion Tests," *IMechE* (1977) 37-54.
13. Kjeldsen, S. P.: "The Experimental Verification of Numerical Models of Plunging Breakers," *Proceedings Coastal Engineering Conference*, (1984) 15-30.
14. Dommermuth, D. G., Yue, D. K. P., Lin, W. M., Rapp, R. J., Chan, E. S. and Melville, W. K.: "Deep-water Plunging Breakers: A Comparison between Potential Theory and Experiments," *Journal of Fluid Mechanics* (1988) Vol. 189 423-442.
15. Birkinshaw, M., Easson, W. J., Greated, C. A. and Webb, R. M.: "Breaking Wave Design: A Case History," *Proc. Instn. Civil Engineers. Part 2*, (1988) Vol. 85, 415-433.
16 Skjelbreia, J.E.: "Observation of Breaking Waves on Sloping Bottoms by Use of Laser Doppler Velocimetry," *Report No. KH-R-48, California Institute of Technology Pasadena, California*, (May 1987).
17. Davis, M.C. and Zarnick, E.E.: "Testing Ship Models in Transient Waves," *Proc. 5th Symposium on Naval Hydrodynamics*, Bergen, Norway, (September 1964).
18. Durrani, T. S. and Greated, C. A.: *Laser Systems in Flow Measurement*, Plenum, New York City (1977).
19. Durst, F., Melling, A. and Whitelaw, J.H.: *Principles and Practice of Laser Doppler Anemometry*, Academic Press, London (1976).

Table 1. Measured Velocities Under 25 cm TWW

Elevation (cm)*	Distance from Flap (m)						
	21.3	21.4	21.5	21.6	21.7	21.8	21.9
	Horizontal Velocity (m/s)						
14			1.47				
10		0.94	0.64	0.95			
5	0.57	0.62	0.63	0.63	0.66	0.73	
0	0.47	0.40	0.51	0.52	0.50	0.59	0.60
-10	0.13	0.14	0.30	0.34	0.29	0.43	0.41
-20	0.10	0.11	0.23	0.25	0.22	0.33	0.31
-30	0.10	0.13	0.19	0.19	0.18	0.26	0.23
	Vertical Velocity (m/s)**						
14			0.15				
10		-0.30	-0.39	0.05			
5	-0.12	-0.42	-0.42	0.07	-0.03	-0.01	
0	-0.34	-0.36	-0.19	0.08	0.07	0.03	0.11
-10	-0.29	-0.31	-0.29	0.09	0.14	0.01	0.08
-20	-0.25	-0.24	-0.18	0.04	0.09	0.05	0.08
-30	-0.21	-0.20	-0.15	0.02	0.06	0.02	0.08

* negative wave elevation = below SWL
** negative vertical velocity = downward

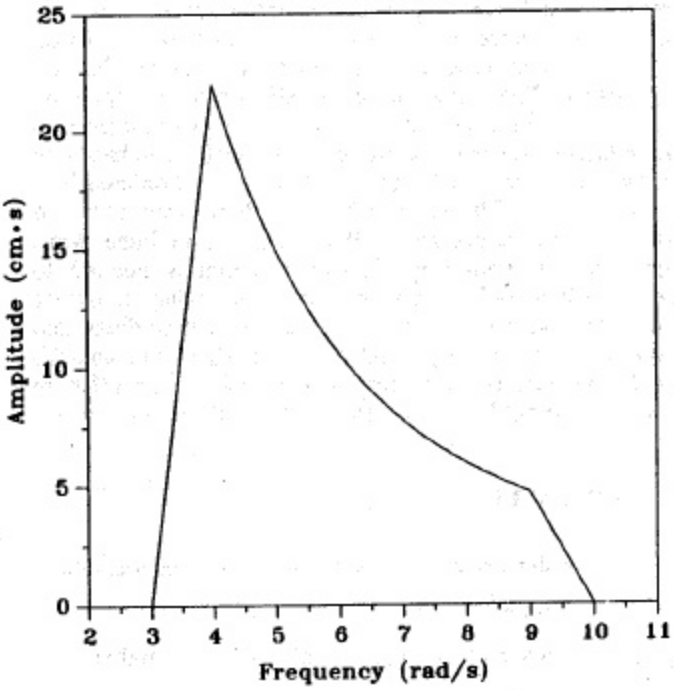

Fig. 1. Fourier Spectrum of Transient Wave

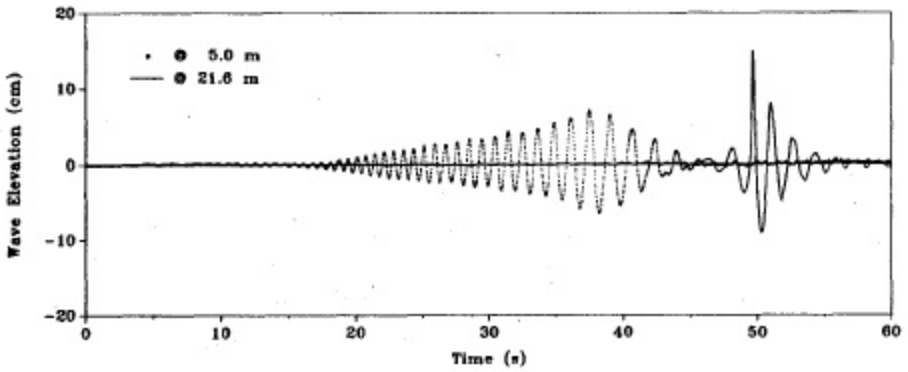

Fig. 2. Measured Extreme Transient Wave Elevation Time Series @ 5 and 21.6 m

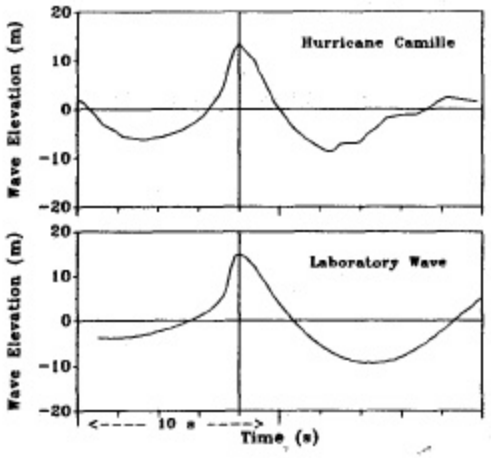

Fig. 3. Time Series of Hurricane Camille and Scaled (1:100) Transient Wave

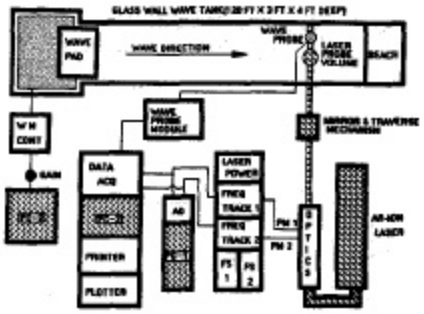

Fig. 4. Schematic of LDA System and Wave Making Facilities (PC-Computer, FS-Frequency Shifter, PM-Photomultiplier, AD-Analog to Digital Interface, WM-Wave Maker)

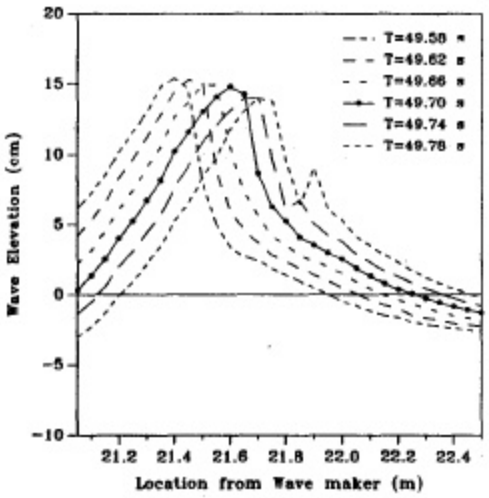

Fig. 5. Measured Transient Wave Profiles in the Vicinity of Focusing Point of 21.6 m

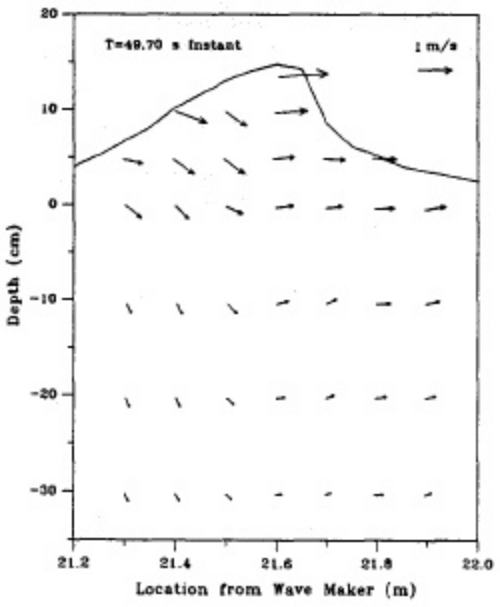

Fig. 6. Extreme Transient Wave Velocity Field

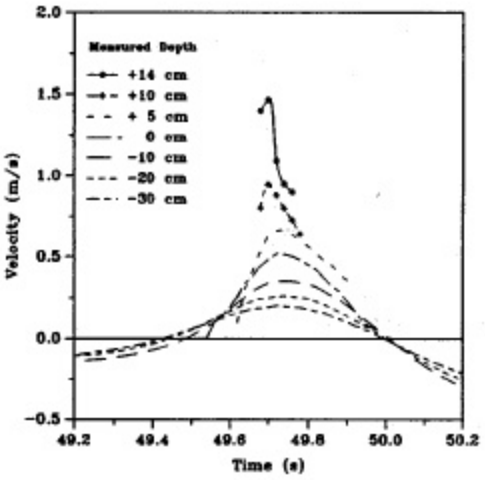

Fig. 7. Horizontal Velocity Time Series for Transient Wave at Various Depths

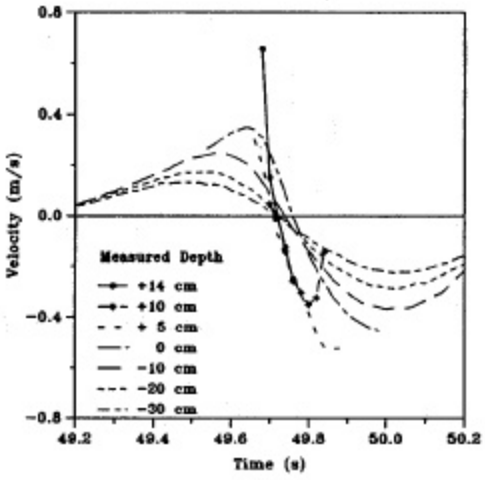

Fig. 8. Vertical Velocity Time Series for Transient Wave at Various Depths

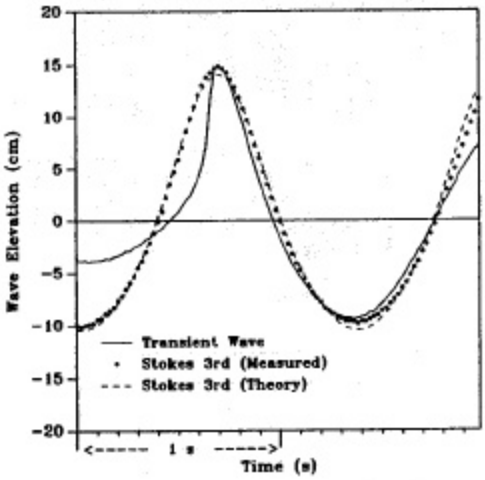

Fig. 9. Elevation Time Series for Extreme Transient and Stokes Waves

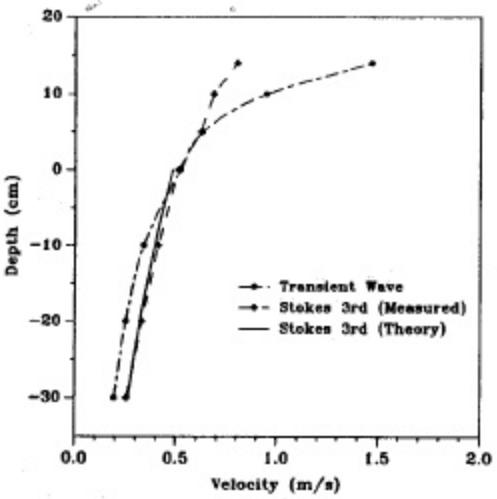

Fig. 10. Horizontal Velocity Under Crest Peak of Transient and Stokes Waves